



**HAL**  
open science

## **Patterning of Superconducting Two-Dimensional Electron Gases based on AlO<sub>x</sub>/KTaO<sub>3</sub> (111) Interfaces**

Hugo Witt, Srijani Mallik, Luis Moreno Vicente-arche, Gerbold Ménard, Guilhem Saïz, Daniela Stornaiuolo, Maria d'Antuono, Isabella Boventer, Nicolas Bergeal, Manuel Bibes

► **To cite this version:**

Hugo Witt, Srijani Mallik, Luis Moreno Vicente-arche, Gerbold Ménard, Guilhem Saïz, et al.. Patterning of Superconducting Two-Dimensional Electron Gases based on AlO<sub>x</sub>/KTaO<sub>3</sub> (111) Interfaces. *Advanced Physics Research*, 2023, 2 (10), pp.2200077. 10.1002/apxr.202200077 . hal-04288425

**HAL Id: hal-04288425**

**<https://hal.science/hal-04288425v1>**

Submitted on 16 Nov 2023

**HAL** is a multi-disciplinary open access archive for the deposit and dissemination of scientific research documents, whether they are published or not. The documents may come from teaching and research institutions in France or abroad, or from public or private research centers.

L'archive ouverte pluridisciplinaire **HAL**, est destinée au dépôt et à la diffusion de documents scientifiques de niveau recherche, publiés ou non, émanant des établissements d'enseignement et de recherche français ou étrangers, des laboratoires publics ou privés.



Distributed under a Creative Commons Attribution 4.0 International License

# Patterning of Superconducting Two-Dimensional Electron Gases based on $\text{AlO}_x/\text{KTaO}_3$ (111) Interfaces

Hugo Witt, Srijani Mallik, Luis Moreno Vicente-Arche, Gerbold Ménard, Guilhem Saiz, Daniela Stornaiuolo, Maria D'Antuono, Isabella Boverter, Nicolas Bergeal, and Manuel Bibes\*

The versatility of properties displayed by two-dimensional electron gases (2DEGs) at oxide interfaces has fostered intense research in hope of achieving exotic electromagnetic effects in confined systems. Of particular interest is the recently discovered superconducting state appearing in (111)-oriented  $\text{KTaO}_3$  interfaces, with a critical temperature  $T_c \approx 2$  K, almost 10 times higher than that of  $\text{SrTiO}_3$ -based 2DEGs. Just as in  $\text{SrTiO}_3$ -based 2DEGs, fabricating devices in this new system is a technical challenge due to the fragility of the 2DEG and the propensity of bulk  $\text{KTaO}_3$  to become conducting outside the devices upon adventitious oxygen vacancy doping. Here, three different techniques are presented for patterning Hall bars in  $\text{AlO}_x/\text{KTaO}_3$  (111) heterostructures. The devices show superconducting transitions ranging from 1.3 to 1.78 K, with limited degradation from the unpatterned thin film, and enable an efficient tuning of the carrier density by electric field effect. The array of techniques allows for the definition of channels with a large range of dimensions for the design of various kinds of devices to explore the properties of this system down to the nanoscale.

serve as the main building block for devices with applications in spintronics,<sup>[5]</sup> orbitronics,<sup>[6–8]</sup> and topological quantum computing.<sup>[9]</sup> Indeed, with a superconducting critical temperature ( $T_c$ ) and a Rashba splitting of an order of magnitude higher in  $\text{KTaO}_3$  (111)<sup>[1,8]</sup> compared to  $\text{SrTiO}_3$ ,<sup>[10–12]</sup> the functional perspectives of this material look promising. However, the discovery and control of the electronic properties of  $\text{KTaO}_3$ -based interfaces, and all the more so of  $\text{KTaO}_3$  (111), are hampered by difficulties in device fabrication. Indeed, on the material side, the  $\text{KTaO}_3$  surface is sensitive, with volatile K cations and O anions that can be lost by annealing, etching or polishing. Regarding processing, the use of classic UV lithography polymer resist during growth is excluded by high temperature steps that are integral parts to the 2DEG formation process.<sup>[13]</sup>

The tunability of transport properties is also limited by the lower dielectric constant of  $\text{KTaO}_3$  than that of  $\text{SrTiO}_3$ .<sup>[14]</sup>

Hitherto, the majority of the studies of  $\text{KTaO}_3$  that show superconductivity have been performed on unpatterned thin film samples.<sup>[1–3,15–17]</sup> Nonetheless, a variety of techniques have been proposed to design Hall bars: wet HCl etching on  $\text{EuO}/\text{KTaO}_3$  (111),<sup>[18,19]</sup> etching on  $\text{YAlO}_3/\text{KTaO}_3$  (111),<sup>[20]</sup> scratching on  $\text{Al}_2\text{O}_3/\text{KTaO}_3$  (111),<sup>[21]</sup> conducting AFM


## Introduction

The study of heterostructures based on  $\text{KTaO}_3$  gained significant interest with the discovery of superconductivity in two-dimensional electron gases (2DEG) at interfaces between  $\text{KTaO}_3$  and various overlayers.<sup>[1–3]</sup> Taking inspiration from the research on  $\text{SrTiO}_3$  interfaces,<sup>[4]</sup>  $\text{KTaO}_3$ -based 2DEGs could

H. Witt, S. Mallik, L. M. Vicente-Arche, I. Boverter, M. Bibes  
 Unité Mixte de Physique  
 CNRS  
 Thales  
 Université Paris-Saclay  
 1 Avenue Augustin Fresnel, Palaiseau 91767, France  
 E-mail: manuel.bibes@cnrs-thales.fr

H. Witt, G. Ménard, G. Saiz, N. Bergeal  
 Laboratoire de Physique et d'Etude des Matériaux  
 ESPCI Paris  
 Université PSL  
 CNRS  
 Sorbonne Université  
 Paris 75005, France

D. Stornaiuolo, M. D'Antuono  
 CNR-SPIN  
 Complesso Monte S. Angelo, Via Cinthia, Napoli 80126, Italy  
 D. Stornaiuolo, M. D'Antuono  
 Dipartimento di Fisica  
 Università di Napoli "Federico II"  
 Complesso Monte S. Angelo, Via Cinthia, Napoli Italy

 The ORCID identification number(s) for the author(s) of this article can be found under <https://doi.org/10.1002/apxr.202200077>

© 2023 The Authors. Advanced Physics Research published by Wiley-VCH GmbH. This is an open access article under the terms of the Creative Commons Attribution License, which permits use, distribution and reproduction in any medium, provided the original work is properly cited.

DOI: 10.1002/apxr.202200077

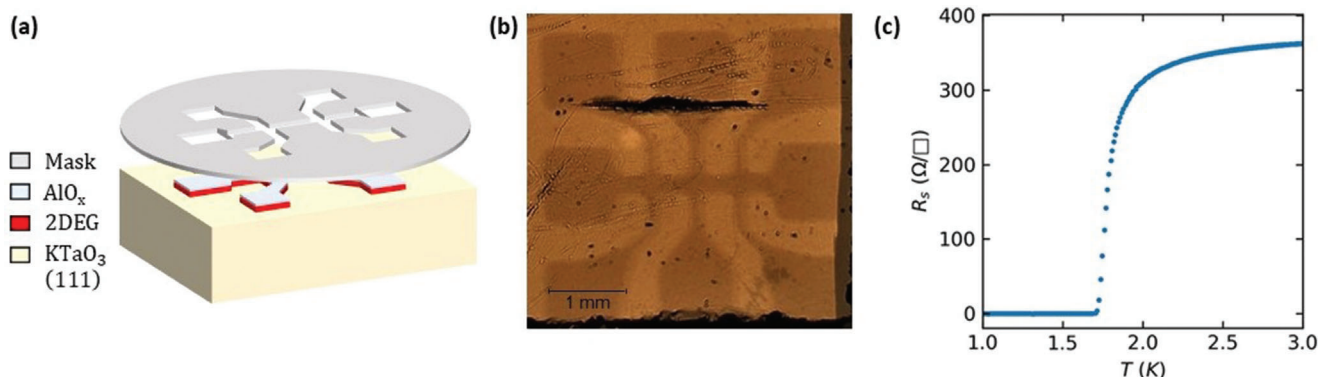


**Figure 1.** Shadow mask method a) Sketch of the fabrication principle. The stainless steel mask is brought as close as possible to the substrate to minimize the shadow effect. b) Optical microscopic view of the 250  $\mu\text{m}$  Hall bar. The horizontal black line is a scratch on the substrate back side used to keep track of the crystallographic orientation of the substrate. c) Low-temperature dependency of the longitudinal resistivity showing the superconducting transition at 1.78 K.

charging<sup>[22]</sup> and ultra-low voltage electron beam lithography<sup>[22]</sup> as well as using a thick amorphous  $\text{Al}_2\text{O}_3$  hard mask deposited by pulsed laser deposition<sup>[2]</sup> on  $\text{LaAlO}_3/\text{KTaO}_3$  (111) and  $\text{LaAlO}_3/\text{KTaO}_3$  (110), or resorting to ionic liquid gating on  $\text{KTaO}_3$  (111).<sup>[23]</sup>

In this study, we report the fabrication of Hall bars in superconducting  $\text{KTaO}_3$  (111) 2DEGs patterned employing three methods: (i) stainless steel shadow masking, (ii)  $\text{Ar}^+$  beam milling at cryogenic temperature, and (iii) using an insulating  $\text{Al}_2\text{O}_3$  hard mask deposited by sputtering. Combined with a simple Al metal deposition method to create the 2DEG,<sup>[3]</sup> these patterning recipes may be easily implemented using classic lithography capabilities. We demonstrate a fine tuning control of the carrier density by electric field effect, modulated by the width of the channel.

## Results

For all samples, the 2DEG was formed by growing a 1.8 nm Al film at 500 °C in Ar atmosphere at  $6 \times 10^{-4}$  mbar by DC magnetron sputtering system (PLASSYS MP450S), as described in Ref. [3], with substrates supplied by MTI corporation. The characterisation was conducted by optical and atomic force microscopy, preliminary transport measurements were done in a Quantum Design Dynacool system and low temperature transport measurements in a dilution refrigerator from 30 mK to 300 K. For the transport measurements, contact was made by wire bonding on the contact pads.

The first method we employed to pattern a Hall bar on  $\text{KTaO}_3$  (111) substrates was shadow masking with a stainless steel mask. The advantage of this technique is the possibility to minimize the chemical impact on the surface of the as-received substrate. However, the dimensions of the features are limited by the resolution of the steel cutting technique.

We used a 150  $\mu\text{m}$  thick laser cut stainless steel mask in a 4 mm x 4 mm design of a 250  $\mu\text{m}$  wide and 2 mm long Hall bar, mounted *ex situ* on the substrate plate without prior treatment to the substrate. A thin layer of Al was then sputtered on the  $\text{KTaO}_3$  substrate, as described in Figure 1a and Ref. [3]. The shadow effect is negligible compared with the dimensions of the device and channels are well defined (Figure 1b). Atomic force

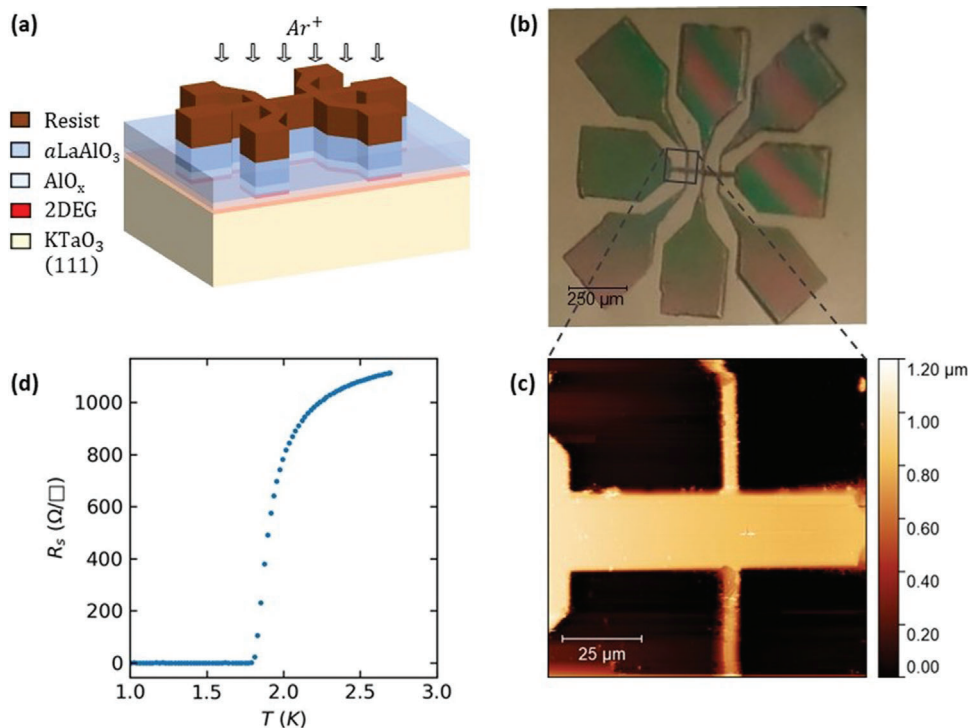
microscopy (not shown) revealed a smooth surface on the Hall bar, comparable to thin film samples. X-ray photoelectron spectroscopy showed no contamination by the mask.

Figure 1c displays the low-temperature dependence of the sheet resistance. We observe a metallic behavior characteristic of a 2DEG, with a superconducting transition at  $T_c \approx 1.78$  K, replicating the behaviour of an unpatterned thin film.<sup>[3]</sup>

The second method yielding a superconducting 2DEG channel at the  $\text{AlO}_x/\text{KTaO}_3$  (111) interface is liquid  $\text{N}_2$ -cooled argon ion beam etching. Ion beam etching is seldom used to pattern 2DEG-hosting interfaces due to the formation of oxygen vacancies at the substrate's surface upon ion irradiation.<sup>[24,25]</sup> The vacancies dope the substrate with electrons, shunting the 2DEG in transport.  $\text{KTaO}_3$  is analogous to  $\text{SrTiO}_3$  in this regard.<sup>[26]</sup> To avoid this effect on the  $\text{LaAlO}_3/\text{SrTiO}_3$  system, a low energy ion beam can be used to suppress conductivity by turning the  $\text{LaAlO}_3$  amorphous without physically etching it, avoiding  $\text{SrTiO}_3$  irradiation.<sup>[27]</sup> Another approach consists in reducing the kinetics of the oxygen vacancy formation and diffusion out of the sample by cooling it with liquid nitrogen during the ion beam etching.<sup>[28]</sup> The sides of the devices thus fabricated are free, and could couple in-plane to subsequently grown complex materials such as conventional superconductors. Using this technique, a pattern resolution of 160 nm could be reached.<sup>[28]</sup>

Here, a thin film of Al was sputtered on a (111)-oriented  $\text{KTaO}_3$ , then oxidized to  $\text{AlO}_x$  in air, and subsequently capped by a 10 nm thick protective layer of amorphous  $\text{LaAlO}_3$  grown by pulsed laser deposition in  $\text{O}_2$  atmosphere at  $1 \times 10^{-6}$  mbar. We then patterned the sample by UV lithography to form 25  $\mu\text{m}$  wide Hall bars. The resist used was SPR 700 1.0, developed with MF-319, creating a 1.1  $\mu\text{m}$  thick resist mask on top of the 2DEG. The system was then etched by a low-intensity Ar ion beam with a current of 5 mA and beam voltage of 315 V with the pressure in the chamber at  $1 \times 10^{-4}$  mbar, resulting in an etching rate of 1 nm  $\text{s}^{-1}$ . During etching, the sample was glued to a cold finger kept at 77 K. Testing the resistance of the etched surface immediately after etching confirmed the absence of conductivity outside of the devices.

Optical and AFM microscopy confirms the structural integrity of the channels thus defined down to 5  $\mu\text{m}$  for the contact



**Figure 2.**  $\text{Ar}^+$  beam milling method a) Sketch of the sample in the final step of fabrication. The transparent layers, not protected by the resist pattern, are etched during the low-temperature milling process, down to a few nanometers into the bare substrate. b) Optical and c) atomic force microscopic view of the 25  $\mu\text{m}$  Hall bar. d) Low-temperature dependance of the longitudinal resistance showing the superconducting transition at 1.8 K.

channels on the measured samples (Figure 2b,c), only limited by the precision of the UV lithography.

The device has a characteristic behavior of a metallic 2DEG where the resistance decreases with the temperature. At low temperature, the resistivity measurements show a superconducting transition at  $T_c \approx 1.8 \text{ K}$  (Figure 2d), identical to the  $T_c$  obtained for a thin film.<sup>[3]</sup>

The third approach is based on the method developed by Schneider *et al.*<sup>[29]</sup> and consists in restricting the surface available for 2DEG formation by first patterning a hard mask on the sample using UV lithography. The desired design for the device is patterned in resist, directly on the substrate. A layer of insulating material is then grown on the sample at room temperature, such that, after lift-off, it forms a template for the 2DEG to be grown onto (Figure 3a). This hard mask then prevents the formation of a conducting layer outside of the pattern. Versatile insulators can be used as hard mask such as  $\text{MgO}$ , amorphous  $\text{LaAlO}_3$  or  $\text{Al}_2\text{O}_3$ , using different deposition techniques including magnetron sputtering or pulsed laser deposition, in conditions ensuring that no conducting layer forms in the substrate underneath. This technique allows the use of simple UV lithography and lift-off processes despite the high temperature annealing and growth. Another advantage is the possibility to see the devices with the naked eye thanks to the contrast between the thick opaque hard mask layer and the thin and transparent conducting regions. However, the contact between the  $\text{KTaO}_3$  surface and the resist prior to the growth of the 2DEG may degrade the quality of the substrate surface, despite cleaning and annealing steps following the lift-off, as opposed to a deposition on a fresh substrate.

For this third method, we patterned the  $\text{KTaO}_3$  sample with resist using the negative image of the mask that was used for the ion beam etching method. A 50 nm thick layer of amorphous  $\text{Al}_2\text{O}_3$  was sputtered with 30 W power in a  $5 \times 10^{-4}$  mbar Ar atmosphere. After lift-off, Al was sputtered on the sample with the same recipe as the other patterning techniques. The Al in contact with the substrate, in the areas not covered by the hard mask, forms the 2DEG, while the film deposited on the hard mask gets oxidized by the oxide insulator itself and by air *ex situ*. We verified that there was no conducting metallic Al bridge between devices over the mask, that would induce leakage.

Microscopic imaging (Figure 3b) shows a large contrast between the amorphous  $\text{Al}_2\text{O}_3$  hard mask and the transparent 2DEG device. The AFM scan (Figure 3c) of the 10  $\mu\text{m}$  wide channel reveals a smooth surface for both the hard mask and the  $\text{AlO}_x/\text{KTaO}_3$  interface and confirms the good definition of the 5  $\mu\text{m}$  wide contact channels. We performed temperature dependent resistance measurement to assess superconductivity, confirming the 2D nature of the conducting layer with the characteristic metallic behaviour, and the transition at  $T_c \approx 1.3 \text{ K}$  (Figure 3d).

We conducted Hall measurements on all three samples while applying a back gate voltage. The Hall effect was linear for all samples at all gate voltages. We extracted the carrier density assuming a single type of carriers.<sup>[30]</sup> All samples had carrier densities of about  $6 \times 10^{13} \text{ cm}^{-2}$  in the virgin state at 2 K, before any gate application. The mobilities were in the 130 – 250  $\text{cm}^2 \text{ V}^{-1} \text{ s}^{-1}$  range at 2 K, which is in the high range of reported values.<sup>[1,16,17,20,21,31]</sup>

Figure 4 shows the gate dependency of the carrier density for the

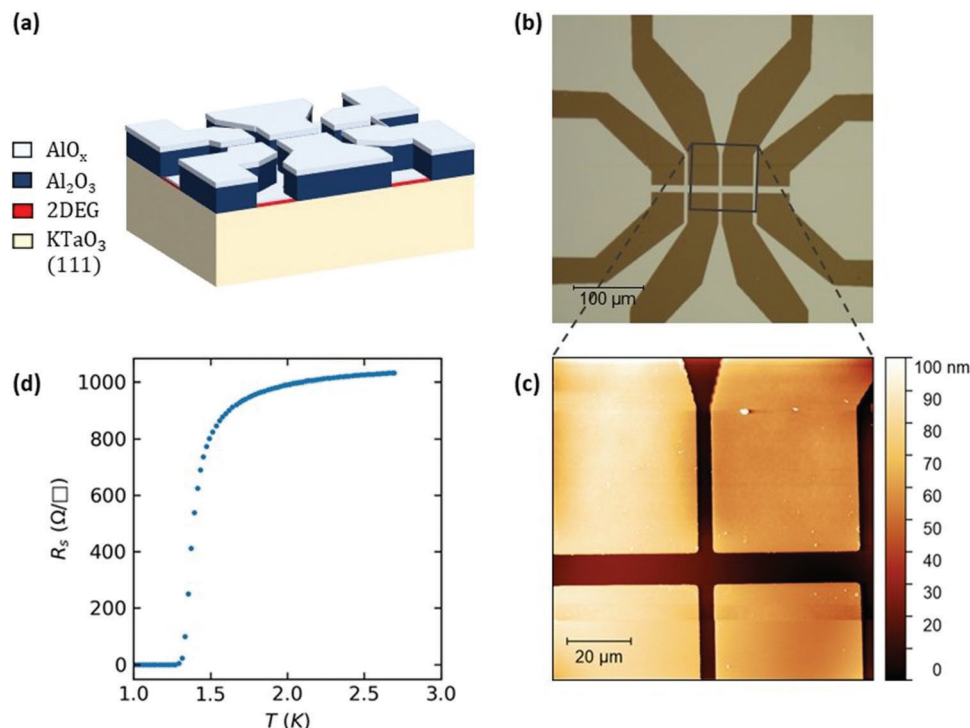


**Figure 3.** Hard mask method a) Sketch of the sample in the final state of fabrication. The  $\text{AlO}_x$  layer topping the  $\text{Al}_2\text{O}_3$  hard mask is the layer of metallic Al, deposited together with what forms the 2DEG at the interface, that oxidizes in an insulating layer in contact with the mask. b) Optical and c) atomic force microscopic view of the  $10\ \mu\text{m}$  Hall bar. d) Low-temperature dependency of the longitudinal resistance showing the superconducting transition at 1.3 K.

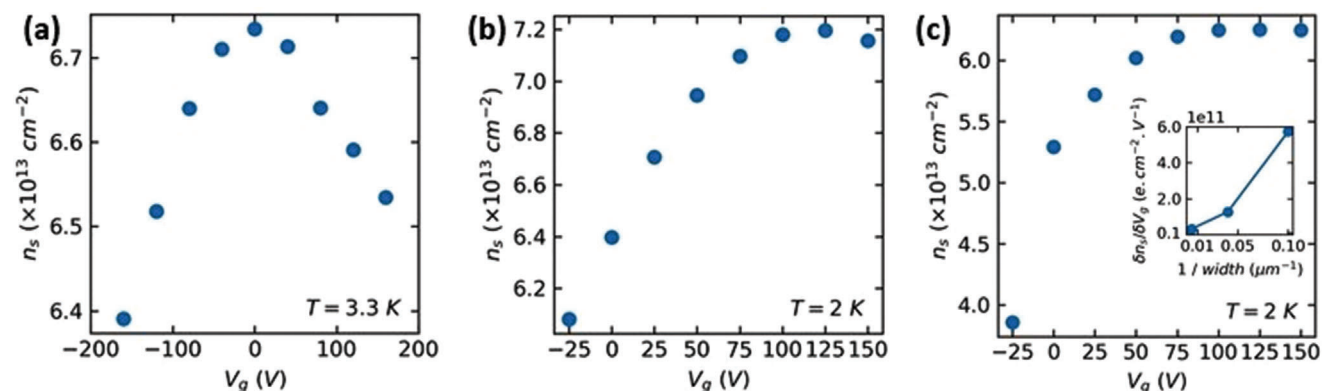


**Figure 4.** Carrier density tuning. Field effect carrier density modulation from Hall measurements with a back gate voltage, assuming a single type of charge carriers, of the three samples presented : a)  $250\ \mu\text{m}$  wide Hall bar deposited by shadow mask, b)  $25\ \mu\text{m}$  wide Hall bar etched at low temperature, c)  $10\ \mu\text{m}$  wide Hall bar in an amorphous  $\text{Al}_2\text{O}_3$  hard mask. (inset) Dependency of the maximum gradient of carrier density modulation with the inverse of the width, for the three devices studied.

three samples. The amplitude of the carrier density modulation is inversely proportional to the channel width, varying over the explored gate voltage range by  $0.34 \times 10^{13}\ \text{cm}^{-2}$  in a  $250\ \mu\text{m}$  wide channel made by the shadow mask method,  $1.11 \times 10^{13}\ \text{cm}^{-2}$ , that is, one order of magnitude higher in a  $25\ \mu\text{m}$  wide channel made by low-temperature etching and  $3.43 \times 10^{13}\ \text{cm}^{-2}$  in a  $10\ \mu\text{m}$  wide channel in an insulating hard mask. As shown in the inset in Figure 4c, the field effect efficiency, defined as the maximum of the gradient of the carrier density dependency on gate voltage, increases proportionally with the inverse of the channel

width. This is consistent with Ref. [32], who showed that the capacitance per area is inversely proportional to the geometrical size of the bar since here the length of the channel is the same for all devices.

## Conclusion

In conclusion, we have shown that efficient field effect control of the carrier density in a superconducting 2DEG formed at the

$\text{AlO}_x/\text{KTaO}_3$  (111) interface may be achieved using accessible fabrication methods: with a stainless steel shadow mask using no chemical surface treatment, and making use of classic UV lithography techniques in combination with ion beam milling at low temperature or deposition of an insulating hard mask. These fabrication techniques may help design more complex devices to control and harness the properties of the superconducting phase of the interface.

## Acknowledgements

This work was supported by the ANR QUANTOP Project-ANR-19-CE470006 grant, by the QuantERA ERA-NET Cofund in Quantum Technologies (Grant Agreement No. 731473) implemented within the European Union's Horizon 2020 Program (QUANTOX). We thank Marco Salluzzo for useful comments.

## Conflict of Interest

The authors declare no conflict of interest.

## Data Availability Statement

The data that support the findings of this study are available from the corresponding author upon reasonable request.

## Keywords

field-effect devices,  $\text{KTaO}_3$ , oxide interfaces, superconductivity, two-dimensional electron gas

Received: October 25, 2022

Revised: February 17, 2023

Published online: April 25, 2023

- [1] C. Liu, X. Yan, D. Jin, Y. Ma, H.-W. Hsiao, Y. Lin, T. M. Bretz-Sullivan, X. Zhou, J. Pearson, B. Fisher, J. S. Jiang, W. Han, J.-M. Zuo, J. Wen, D. D. Fong, J. Sun, H. Zhou, A. Bhattacharya, *Science* **2021**, *371*, 716.
- [2] Z. Chen, Y. Liu, H. Zhang, Z. Liu, H. Tian, Y. Sun, M. Zhang, Y. Zhou, J. Sun, Y. Xie, *Science* **2021**, *372*, 721.
- [3] S. Mallik, G. C. Ménard, G. Saiz, H. Witt, J. Lesueur, A. Gloter, L. Benfatto, M. Bibes, N. Bergeal, *Nat. Commun.* **2022**, *13*, 4625.
- [4] Y.-Y. Pai, A. Tylan-Tyler, P. Irvin, J. Levy, *Rep. Prog. Phys.* **2018**, *81*, 036503.
- [5] F. Trier, P. Noël, J.-V. Kim, J.-P. Attané, L. Vila, M. Bibes, *Nat. Rev. Mater.* **2022**, *7*, 258.
- [6] A. Johansson, B. Göbel, J. Henk, M. Bibes, I. Mertig, *Phys. Rev. Res.* **2021**, *3*, 013275.
- [7] L. M. Vicente-Arche, J. Bréhin, S. Varotto, M. Cosset-Cheneau, S. Mallik, R. Salazar, P. Noël, D. C. Vaz, F. Trier, S. Bhattacharya, A. Sander, P. Le Fèvre, F. Bertran, G. Saiz, G. Ménard, N. Bergeal, A. Barthélémy, H. Li, C.-C. Lin, D. E. Nikonov, I. A. Young, J. E. Rault, L. Vila, J.-P. Attané, M. Bibes, *Adv. Mater.* **2021**, *33*, 2102102.
- [8] S. Varotto, A. Johansson, B. Göbel, L. M. Vicente-Arche, S. Mallik, J. Bréhin, R. Salazar, F. Bertran, P. L. Fèvre, N. Bergeal, J. Rault, I. Mertig, M. Bibes, *Nat. Commun.* **2022**, *13*, 6165.
- [9] A. Barthelemy, N. Bergeal, M. Bibes, A. Caviglia, R. Citro, M. Cuoco, A. Kalaboukhov, B. Kalisky, A. Perroni, J. Santamaria, D. Stornaiuolo, M. Salluzzo, *EPL* **2021**, *133*, 17001.
- [10] N. Reyren, S. Thiel, A. D. Caviglia, L. F. Kourkoutis, G. Hammerl, C. Richter, C. W. Schneider, T. Kopp, A.-S. Rütschi, D. Jaccard, M. Gabay, D. A. Muller, J.-M. Triscone, J. Mannhart, *Science* **2007**, *317*, 1196.
- [11] A. D. Caviglia, M. Gabay, S. Gariglio, N. Reyren, C. Cancellieri, J.-M. Triscone, *Phys. Rev. Lett.* **2010**, *104*, 126803.
- [12] D. C. Vaz, F. Trier, A. Dyrdal, A. Johansson, K. Garcia, A. Barthélémy, I. Mertig, J. Barnas, A. Fert, M. Bibes, *Phys. Rev. Mater.* **2020**, *4*, 071001.
- [13] P. Krantz, A. Tyner, P. Goswami, V. Chandrasekhar, *ArXiv:2209.10534* **2022**.
- [14] S. H. Wemple, *Phys. Rev.* **1965**, *137*, A1575.
- [15] A. H. Al-Tawhid, J. Kanter, M. Hatefipour, D. P. Kumah, J. Shabani, K. Ahadi, *J. Elect. Mater.* **2021**, *51*, 6305.
- [16] C. Liu, X. Zhou, D. Hong, B. Fisher, H. Zheng, J. Pearson, D. Jin, M. R. Norman, A. Bhattacharya, *Nat. Commun.* **2022**.
- [17] Y. Sun, Y. Liu, W. Pan, Y. Xie, *J. Phys.: Condens. Matter.* **2022**, *34*, 444004.
- [18] Y. Ma, J. Niu, W. Xing, Y. Yao, R. Cai, J. Sun, X. C. Xie, X. Lin, W. Han, *Chinese Phys. Lett.* **2020**, *37*, 117401.
- [19] W. Qiao, Y. Ma, J. Yan, W. Xing, Y. Yao, R. Cai, B. Li, R. Xiong, X. C. Xie, X. Lin, W. Han, *Phys. Rev. B* **2021**, *104*, 184505.
- [20] G. Zhang, L. Wang, J. Wang, G. Huang, H. Xue, Y. Wu, Y. Song, Z. An, C. Zheng, J. Li, Y. Chen, W. Li, *ArXiv:2111.05650* **2021**.
- [21] S. K. Ojha, P. Mandal, S. Kumar, S. Middey, *ArXiv:2206.10361* **2022**.
- [22] M. Yu, C. Liu, D. Yang, X. Yan, Q. Du, D. D. Fong, A. Bhattacharya, P. Irvin, J. Levy, *Nano Lett.* **2022**, *22*, 6062.
- [23] T. Ren, M. Li, X. Sun, L. Ju, Y. Liu, S. Hong, Y. Sun, Q. Tao, Y. Zhou, Z.-A. Xu, Y. Xie, *Sci. Adv.* **2022**, *8*, eabn4273.
- [24] D. Kan, T. Terashima, R. Kanda, A. Masuno, K. Tanaka, S. Chu, H. Kan, A. Ishizumi, Y. Kanemitsu, Y. Shimakawa, M. Takano, *Nat. Mater.* **2005**, *4*, 816.
- [25] G. Herranz, O. Copie, A. Gentils, E. Tafra, M. Basletic, F. Fortuna, K. Bouzehouane, S. Fusil, A. Jacquet, C. Carrétéro, M. Bibes, A. Hamzic, A. Barthélémy, *J. Appl. Phys.* **2010**, *107*, 103704.
- [26] S. K. Ojha, S. K. Gogoi, P. Mandal, S. D. Kaushik, J. W. Freeland, M. Jain, S. Middey, *Phys. Rev. B* **2021**, *103*, 085120.
- [27] P. Paolo Aurino, A. Kalaboukhov, N. Tuzla, E. Olsson, T. Claeson, D. Winkler, *Appl. Phys. Lett.* **2013**, *102*, 201610.
- [28] M. D'Antuono, A. Kalaboukhov, R. Caruso, S. Wissberg, S. Weitz Sobelman, B. Kalisky, G. Ausanio, M. Salluzzo, D. Stornaiuolo, *Nanotechnology* **2022**, *33*, 085301.
- [29] C. W. Schneider, S. Thiel, G. Hammerl, C. Richter, J. Mannhart, *Appl. Phys. Lett.* **2006**, *89*, 122101.
- [30] F. Y. Bruno, S. M. Walker, S. Ricci, A. de la Torre, Z. Wang, A. Tamai, T. K. Kim, M. Hoesch, M. S. Bahramy, F. Baumberger, *Adv. Electron. Mater.* **2019**, *5*, 1800860.
- [31] Y. Liu, Z. Liu, M. Zhang, Y. Sun, H. Tian, Y. Xie, *ArXiv:2208.05712* **2022**.
- [32] D. Rakhmilevitch, I. Neder, M. Ben Shalom, A. Tsukernik, M. Karpovskii, Y. Dagan, A. Palevski, *Phys. Rev. B* **2013**, *87*, 125409.